Harnessing programmed holes in hydrogel bilayers to design soft self-folding machines

Meie Li , Zongling Jiang , Ning An , Jinxiong Zhou

PII: S0020-7403(17)33453-7
DOI: 10.1016/j.ijmecsci.2018.03.011
Reference: MS 4221

To appear in: *International Journal of Mechanical Sciences*

Received date: 4 December 2017
Revised date: 24 February 2018
Accepted date: 12 March 2018

Please cite this article as: Meie Li , Zongling Jiang , Ning An , Jinxiong Zhou , Harnessing programmed holes in hydrogel bilayers to design soft self-folding machines, *International Journal of Mechanical Sciences* (2018), doi: 10.1016/j.ijmecsci.2018.03.011

Harnessing programmed holes in hydrogel bilayers to design soft self-folding machines

Meie Li[1], Zongling Jiang[1], Ning An[2] and Jinxiong Zhou[2, a)]

[1] State Key Laboratory for Mechanical Behavior of Materials, School of Materials Science and Engineering, Xi'an Jiaotong University, Xi'an 710049, China

[2] State Key Laboratory for Strength and Vibration of Mechanical Structures, Shaanxi Engineering Laboratory for Vibration Control of Aerospace Structures, School of Aerospace, Xi'an Jiaotong University, Xi'an 710049, China

Abstract: We present a physics-based finite element simulation of self folding of a hydrogel bilayer with programmed holes. Introducing holes in a bilayer modifies the topology and boundary of the bilayer. Early state swelling of a hydrogel bilayer forms rolled tubes along the periphery of the bilayer and adds the local rigidity along the boundary. Our numerical simulation shows that formation of rolled edges switches the deformation mode of hydrogel bilayer from slow and gradual bending to fast and sudden buckling or folding. On demand folding is thus possible by tuning the location, size and shape of holes. The uncovered folding mechanism is leveraged to design a number of soft self-folding machines. The results throw light on design and simulation of soft self-folding machines.

Key words: hydrogel, self-folding, buckling, programmed holes, finite element method

Corresponding author: a) jxzhouxx@mail.xjtu.edu.cn

1. Introduction

Folding has evolved from an aesthetic paper game to a modern technology for functional materials and structures across scales: from molecular scale DNA to very large scale deployable aerospace structures such as solar sails and panels.[1-5] More recently, there has been an upsurge of interests to develop folding in particular self-folding technologies to fabricate multifunctional materials, transforming architectures, robots, and self-folding machines.[1-5] Merits of using self-folding technology to fabricate morphing materials and structures include compact storage, invasive manipulation and remote control, and reduction of manufacture complexity, etc.

Smart active materials, such as shape memory alloys (SMA),[3] shape memory polymers (SMP),[6] polymer gels,[7-10] temperature or light-sensitive polymers,[11,12] and dielectric elastomers (DE) [13-15] are leveraged to design and fabricate self-folding structures. Among them, stimuli-responsive hydrogels are ideal candidates for self-folding purpose due to their unique features like sensitivity to diverse stimuli, considerable shape or volume variation, excellent bio-compatibility and bio-degradability.

An elegant example of hydrogel-actuated self-folding structure is a hydrogel bilayer by laminating an inert hydrophobic polymer film on a piece of stimulus-responsive hydrogel sheet. Upon variation of environmental stimulus, the hydrogel layer swells or shrinks but the inert layer does not, causing mismatch in strains of the two layers and resulting in bending of the bilayer. Hydrogel bilayers may be fabricated as beams, plates or simply hinges entrapped in a film. This approach of reversible self-folding of 2D structures into 3D structures has found

diverse applications, ranging from drug delivery, controlled encapsulation, tissue scaffolds, and adaptive optics [7-12]. This basic design using hydrogel bilayers has recently been extended into a trilayer structure, where the hydrogel is sandwiched between two inert stiff layers with patterned openings for mountain and valley folds assignment [8]. This trilayer structure design expands the feasibility of origami-inspired structures, and very complicated folding patterns such as Randlett's flapping bird has been successfully demonstrated using a temperature-sensitive Poly(N-isopropl acrylamide-co-sodium acrylate) (PNIPAM) copolymer.

Despite the success of folding hydrogel bilayers into 3D structures across various scales, the above-mentioned technique is diffusion-limited, meaning that the self-folding is dictated by the diffusion process of water molecules through the hydrogel sample and is relatively slow in seconds or even hours. Very recently, Stoychev et al. [17] proposed a simple way to reduce the response time of self-folding of hydrogel bilayers by introducing hollow holes. A 400×400μm square bilayer with a square hole self-folds in about 20 ms, which is much faster than the swelling of the trilayer which occurs roughly 10 minutes [8]. It should be noted that the bilayer adopted by Stoychev et al. [17] is attached to a solid substrate such as Si wafer or glass. The water-impermeable substrate and the top hydrophobic inert layer hinder the diffusion of water molecules through the thickness of the bilayer, and water can only diffuse laterally in the bilayer, which is identical to that takes place in the trilayer composites.

Introducing holes into hydrogel bilayers gives not only a novel geometric control over the folding fate of the films but also adds the ability to tune the rate of folding, through the careful selection of hole size, location, and shape [17]. The underlying mechanics behind this

phenomenon lies in the fact that the inhomogeneous swelling of hydrogel bilayers firstly results in rolling of the periphery of the film, which stiffens the boundary locally and dramatically affects the subsequent morphing process. In sharp contrast to the swelling-induced gradual increase of curvature throughout the whole bilayer without holes, further swelling of the bilayer with holes builds up more stress until a buckling occurs and the bilayer folds quickly, switching the folding process from slow bending to very fast buckling or snapping.

To elucidate the folding mechanism of the hydrogel bilayers with programmed holes, we present here the finite element modeling of hydrogel bilayers with programmed holes, which is in line with our previous efforts of development and adoption of physics-based model to simulate the self-folding of hydrogel bilayers and trilayers [9,16]. This method avoids the introduction of non-physical parameters such as the thermal expansion coefficient needed in a thermal expansion analogy approach [17]. Several experimental examples were modeled with the folding scenarios captured successfully. We then exploit the novel folding mechanism of hydrogel bilayers and demonstrate some possible soft self-folding machines. The results would aid the design and fabrication of hydrogel-based soft machines.

2. Theory and numerical implementation

In line with the nonlinear field theory for the coupled diffusion and large deformation of hydrogels [18-19], the theory of modeling chemically sensitive hydrogels starts with writing out the free energy of the system. The hydrogel is an aggregate of solid polymer network and a large number of solvent molecules and macroscopically a solid, but microscopically it is a liquid in the sense that all the long chain polymer molecules and the small solvent molecules are mobile.

Defining nominal concentration, *C*, as the number of solvent molecules per unit dry polymer volume, the mixing of polymer molecules and small solvent molecules gives to mixing energy, which is described by the Flory-Rehner model as [18]

$$W_{mix}(C) = -\frac{k_B T}{v}\left[vC\log\left(1+\frac{1}{vC}\right)+\frac{\chi}{1+vC}\right], \quad (1)$$

where k_B is the Boltzmann constant, T is temperature and taken as a constant in this paper, and v is the volume of a solvent molecule, and χ is the Flory polymer-solvent interaction coefficient. The first term inside the bracket comes from the entropy of mixing, while the second term from the enthalpy of mixing.

Migrating of small solvent molecules from the outside environment into the hydrogel not only changes the concentration and mixing process of polymer and solvent, but also makes the crosslinked polymer network stretched, which gives rise to the elastic energy [18,19]

$$W_{ela}(\mathbf{F}) = \frac{1}{2}Nk_B T(F_{iK}F_{iK} - 3 - 2\log\det\mathbf{F}). \quad (2)$$

Here $\mathbf{F}$ is the deformation gradient tensor, and N is the number of chains divided by dry polymer volume. We take the simplest incompressible neo-Hookean hyperelastic model to approximate the elastic energy and of course other forms of hyperelastic models can also be used.

The energy contributions from Equation (1) and (2) amount to the total energy of the hydrogel, $\hat{W}(\mathbf{F},C) = W_{mix}(C) + W_{ela}(\mathbf{F})$, which has two independent field variables, $\mathbf{F}$ and C. However, there is a constraint between the two filed variables, i.e., the so-called molecular incompressibility conditions [20],

$$\det \mathbf{F} = J = 1 + Cv. \quad (3)$$

This ideal condition assumes that all molecules in a gel are incompressible, and the volume of the gel is the sum of the volume of polymer network and the volume of solvents [20]. In numerical practice, it is, however, more convenient to replace concentration C by chemical potential of solvent μ as a field variable. To this end, a Legendre transformation, $W(\mathbf{F}, \mu) = \hat{W}(\mathbf{F}, C) - \mu C$, is introduced. Noting the first invariant of right Cauchy-Green deformation tensor $I_1 = F_{iK}F_{iK}$, and replacing C in Equation (1) by $(J - 1)/v$, the total Helmholtz free energy density of the hydrogel is thus derived as [20]

$$W(I_1, J, \mu) = \frac{1}{2} N k_B T (I_1 - 3 - 2\log J) - \frac{k_B T}{v}\left[(J - 1)\log\frac{J}{J - 1} + \frac{c}{J}\right] - \frac{\mu}{v}(J - 1). \quad (4)$$

This replacement is mathematically equivalent but is helpful for the programming. The last term in Equation (4) is equal to μC, which is the work done by the chemical potential.

We make recourse to commercial finite element software, ABAQUS, and adopt the user subroutine UHYPER for chemically sensitive hydrogels, which was developed by Hong et al. [20]. Implementation of UHYPER is straightforward, being only derivatives of free energy with respect to I_1 and J are needed, which is evaluated readily as

$$\frac{\partial W}{\partial I_1} = \frac{1}{2} N k_B T, \quad (5)$$

$$\frac{\partial W}{\partial J} = -N k_B T / J - \frac{k_B T}{v}\left[\log\frac{J}{J - 1} - \frac{1}{J} - \frac{c}{J^2}\right] - \frac{\mu}{v}. \quad (6)$$

With the material law prescribed by Equation (4), various stress forms can be derived readily and the details are omitted herein. In finite element simulation, we vary the ambient chemical

potential of solvent and model the corresponding equilibrium swelling states of a hydrogel due to our concern. We ignore the kinetic process involved in the swelling phenomena, which is far more complicated problem and tenable by current equilibrium swelling theory.

3. Numerical results and discussions

FIG. 1 shows schematically the hydrogel bilayer of interest in this paper. A non-swollen polymeric film is coated on a piece of stimulus-responsive hydrogel and forms a bilayer, and the bilayer is then attached to a water-impermeable substrate. The top film and the substrate underneath prevent the diffusion of water and it can only migrate laterally into the hydrogel. Initial swelling mainly occurs around the edge of the film and the edge rolls to form a tube. The swollen part of hydrogel detach from the substrate, while the non-swollen part remains flat and attached to the substrate. The formation of the rolled edge or tube adds the rigidity of the local boundary dramatically. In contrast to the swelling-induced bending deformation of a hydrogel bilayer, where the bending curvature increases gradually and prevails the whole system as the bilayer swells, the formation of rolled tubes along the periphery of the bilayer affects the subsequent deformation of the bilayer and changes its deformation from gradual bending to fast buckling. As the bilayer swells, it generates internal stress and the bilayer tends to bend, while the formation of tubes along the periphery tends to flatten the bilayer. The two opposite mechanisms compete with each other and the stored energy in the bilayer continues to increase until the energy barrier for the onset of buckling is overcome and the bilayer folds suddenly.

To numerically validate the above-mentioned folding mechanism of the hydrogel bilayer and elucidate the effect of formation of tubes along the periphery on the following folding deformation, we start with a 10×10×0.2mm model bilayer system given in FIG.2 (a), where the bottom green layer is the stimulus-responsive hydrogel, the top red layer is the inert polymer film, and the black lines are the formed tubes on the edges of the square. To adopt the methodology described previously to model the folding of the hydrogel bilayer with beam-reinforced boundary, we use commercial software, ABAQUS, and the user subroutine UHYPER [20]. We set in our simulation the following parameters: Nv=0.001 and c=0.1. The swelling of hydrogel is regulated by environmental chemical potential. In all our following simulations, we normalize chemical potential by k_BT. At room temperature, k_BT =4×10^{-21}J. For an initial normalized chemical potential η=-0.01, the initial swelling ratio of hydrogel was set to be 1.87888 according to the equilibrium free swelling conditions of hydrogels. The nonswollen polymers and beams were treated as linear elastic materials with Young moduli E=0.03 MPa and E=3 MPa, respectively. The Poisson's ratios for both were set to be 0.3. The hydrogel and the non-swollen polymer are discretized by 3D solid elements C3D8H, and the formed tubes are modeled by beam elements B31. The methodology we adopted is a physics-based approach, so that we can model the swelling process of the hydrogel by varying the environmental chemical potential. FIG. 2(b) shows the simulated folding process of a square hydrogel bilayer with rolled edges under various chemical potentials. To further demonstrate that the swelling-induced deformation of such beam-reinforced hydrogel bilayer is buckling phenomenon, we trace one corner of the square marked in red in the inserted figure and plot its out-of-plane displacement

(z direction, units mm) versus chemical potential. The result is shown in FIG. 2(c). This is a typical buckling load versus displacement curve: below the critical value of the general force, chemical potential herein, the bilayer remains flat and the out-of-plane displacement of the marker is very small; beyond the critical value for the onset of buckling, the bilayer buckles suddenly and the out-of-plane displacement increases steeply. In the simulation of FIG. 2 and the following examples, the degrees of freedom of the central point of the structure were constrained thus the rigid motion of the structure was excluded from the simulation.

The simulation presented in FIG. 2 reproduces the experimental observation reported by Stoychev et al. [17] The early stage of swelling mainly occurs around the boundary or edges of a hydrogel bilayer, and rolled edges form wherever it has a boundary. The rolled tubes along the boundary of the bilayer affect the subsequent folding. A simple way of introducing hollow holes changes the topology of the bilayer and distribution of materials and boundaries. Programmable folding is thus possible by varying the location, size, and shape of holes. To this end, we model a square bilayer with small corner holes as shown in FIG.3. The top panel in FIG. 3 is the schematic of the location of the corner holes, and the bottom panel gives the corresponding folding configurations. For the first two configurations, there are two folding diagonals indicated by the black dashed lines with equal probability. For the rest three configurations, there is only one folding line for each of them and the folding takes place with a predetermined direction. The simulated scenarios presented in FIG.3 also coincide with the experiment by Stoychev et al. [17]

Laying on the basis of understanding of the above-mentioned folding mechanism and exploiting the powerfulness of finite element method, we then move on to the design of novel

soft self-folding machines, which is highlighted by the following numerical examples. FIG. 4 presents the self-folding of a butterfly. FIG. 4(a) gives the geometric design, material distribution and the design of folding lines, which is the core of the design of self-folding machines. One programmed folding line was attained by generating a number of holes along a predetermined path. The holes along the line enhance the stiffness along the line and only folding along line is permitted. FIG. 4(b) gives a series of folding patterns when the environmental chemical potential is changed from -0.01 to -0.03. For designing of self-folding structures, one important source of inspiration is origami-the art and method of paper folding. FIG. 5 shows the origami-inspired self-folding of a paper airplane. This is a typical origami game, and we simulate it to show this can be implemented by hydrogel bilayer structure. The design of the model is presented in FIG. 5(a) with both top view and bottom view. Snapshots in FIG. 5(b) are self-folding deformation for various chemical potentials. Self-folding phenomena are ubiquitous in nature particularly in various plants. Drying of plant leaves and flowers induces diverse folding or curling patterns, which gives insights for the design of self-folding structures. FIG. 6 demonstrates the closing of a multilayer flower. The design is inspired a plant flower, and the folding line is highlighted by the dotted line in FIG. 6(a). Finally, we show that this self-folding mechanism can be leveraged to design soft self-folding machine. The example demonstrated here is a self-folding propeller shown in FIG. 7. The folding line is marked by the dotted line in FIG. 7(a). The folding line is designed and inclined in the middle of the blade such that blades are folded in right-handed direction and anticlockwise. In this example, instead of generating a series of small holes and associated rigid peripheries, a pair of rigid beams with

small gap were added next to the marked folding line. The concept and demonstration of self-folding propeller might be useful for the design of underwater soft robots.

4. Concluding remarks

Shape-changing materials and structures are desirable for broad applications ranging from bioengineering devices, soft actuators, soft machines, batteries, drug vehicles, and deployable aerospace structures. Soft and active materials like hydrogels are ideal candidates for this particular purpose. Ideas of design and fabrication of these shape-changing or self-folding structures stem from deep understanding of morphing or folding mechanism of simple configurations such as bilayer or trilayer structures.

We present a numerical study on the folding mechanism of a hydrogel bilayer with programmed holes. Introducing holes in a bilayer modifies the topology and boundary of the bilayer. Early state swelling of a hydrogel bilayer forms rolled tubes along the periphery of the bilayer and adds the local rigidity along the boundary. On demand folding is possible by tuning the location, size and shape of holes. The formation of rolled edges switches the deformation mode of hydrogel bilayer from slow and gradual bending to fast and sudden buckling or folding. We further demonstrate through several numerical examples that this mechanism can be leveraged to design a number of soft self-folding machines. The numerical tools, basic understanding of folding mechanism along with novel self-folding machines designs would aid the design and control of self-folding machines, and the principles are not limited to hydrogel-based soft machines.

Acknowledgement

This research is supported by Natural Science Foundation of China (grants 11472210 and 11372239).

References

1. Han D, Pal S, Nangreave J, Deng Z, Liu Y, Yan H. DNA origami with complex curvatures in Three-Dimensional space. *Science*. 2011;332:342-346

2. Blees MK, Barnard AW, Rose PA, Roberts SP, McGill KL, Huang PY, Ruyack AR, Kevek JW, Kobrin B, Muller DA, McEuen PL. Graphene kirigami. *Nature*. 2015;524:204

3. Hawkes E, An B, Benbernou NM, Tanaka H, Kim S, Demaine ED, Rus D, Wood RJ. Programmable matter by folding. *P Natl Acad Sci Usa*. 2010;107:12441-12445

4. Silverberg JL, Evans AA, McLeod L, Hayward RC, Hull T, Santangelo CD, Cohen I. Using origami design principles to fold reprogrammable mechanical metamaterials. *Science*. 2014;345:647-650

5. Peraza-Hernandez EA, Hartl DJ, Jr. Malak RJ, Lagoudas DC. Origami-inspired active structures: A synthesis and review. *Smart Mater Struct*. 2014;23

6. Felton S, Tolley M, Demaine E, Rus D, Wood R. A method for building self-folding machines. *Science*. 2014;345:644-646

7. Zheng WJ, An N, Yang JH, Zhou J, Chen YM. Tough

Al-alginate/Poly(N-isopropylacrylamide) hydrogel with tunable LCST for soft robotics. *Acs Appl Mater Inter*. 2015;7:1758-1764

8. Na J, Evans AA, Bae J, Chiappelli MC, Santangelo CD, Lang RJ, Hull TC, Hayward RC. Programming reversibly Self-Folding origami with micropatterned Photo-Crosslinkable polymer trilayers. *Adv Mater*. 2015;27:79-85

9. Guo W, Li M, Zhou J. Modeling programmable deformation of self-folding all-polymer structures with temperature-sensitive hydrogels. *Smart Mater Struct*. 2013;22

10. Silverberg JL, Na J, Evans AA, Liu B, Hull TC, Santangelo CD, Lang RJ, Hayward RC, Cohen I. Origami structures with a critical transition to bistability arising from hidden degrees of freedom. *Nat Mater*. 2015;14:389-393

11. Stoychev G, Turcaud S, Dunlop JWC, Ionov L. Hierarchical Multi-Step folding of polymer bilayers. *Adv Funct Mater*. 2013;23:2295-2300

12. Ionov L. Soft microorigami: Self-folding polymer films. *Soft Matter*. 2011;7:6786-6791

13. Shintake J, Rosset S, Schubert BE, Floreano D, Shea HR. A foldable antagonistic actuator. *Ieee-Asme T Mech*. 2015;20:1997-2008

14. Kofod G, Wirges W, Paajanen M, Bauer S. Energy minimization for self-organized structure formation and actuation. *Appl Phys Lett*. 2007;90

15. Sun W, Liu F, Ma Z, Li C, Zhou J. Soft mobile robots driven by foldable dielectric elastomer actuators. *J Appl Phys*. 2016;120

16. An N, Li M, Zhou J. Predicting origami-inspired programmable self-folding of hydrogel trilayers. *Smart Mater Struct*. 2016;25

17. Stoychev G, Guiducci L, Turcaud S, Dunlop JWC, Ionov L. Hole-Programmed superfast multistep folding of hydrogel bilayers. *Adv Funct Mater*. 2016;26:7733-7739

18. Flory P and Rehner J. Statistical mechanics of cross-linked polymer networks Ⅱ Swelling. J. Chem. Phys. 1943; 11: 521-526.

19. Hong W, Zhao X, Zhou J, Suo Z. A theory of coupled diffusion and large deformation in polymeric gels. *J Mech Phys Solids*. 2008;56:1779-1793

20. Hong W, Liu Z, Suo Z. Inhomogeneous swelling of a gel in equilibrium with a solvent and mechanical load. *Int J Solids Struct*. 2009;46:3282-3289

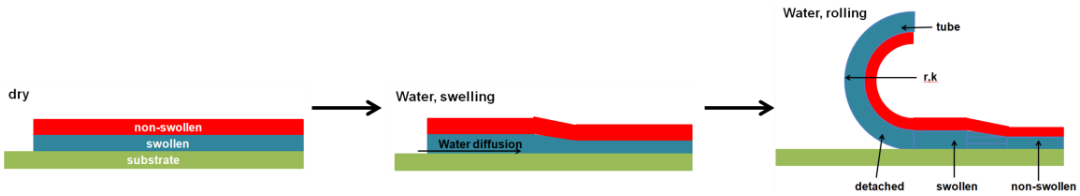

FIG.1 The schematic shows the formation of a rolling edge and tube in a hydrogel bilayer attached to a water impermeable substrate. As water diffuses laterally into the hydrogel, the edge of the film firstly swells and then rolls to form a tube. The swollen part of hydrogel detach from the substrate, while the non-swollen part remains flat and attached to the substrate. The formation of the rolled edge or tube adds the rigidity of the local boundary dramatically.

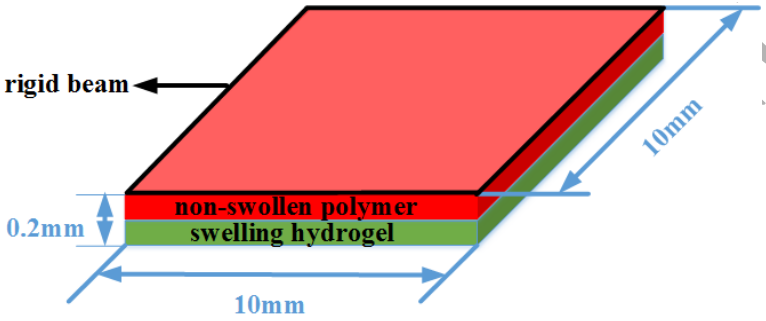

(a)

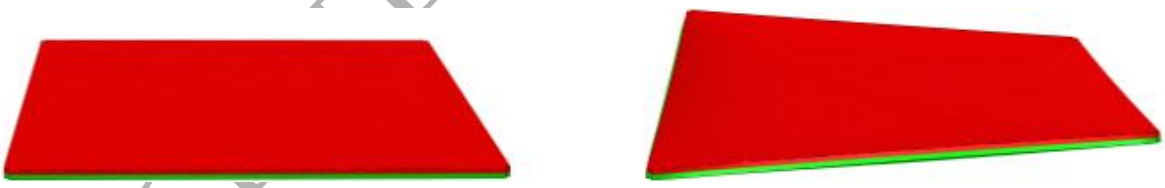

μ= -0.01 μ= -0.00736

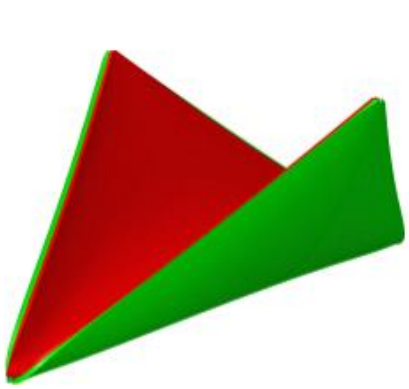

μ= -0.00436

μ= -0.0025

(b)

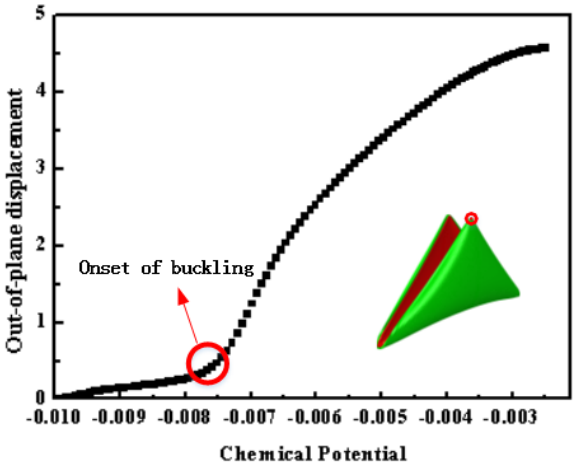

(c)

FIG.2 Buckling-driven self-folding of a 10×10×0.2mm hydrogel bilayer square with rolling edges. (a) Schematic of a hydrogel bilayer square with bottom green layer the stimulus-responsive hydrogel, top red layer the inert polymer film, and black lines the formed tubes on the edges of the square. (b) Simulated self-folding process of the square under various environmental chemical potentials. (c) The out-of-plane displacement (unit mm) of one of the corners of the

square marked in red and inserted in the figure versus chemical potential curve indicates that the folding is a buckling-driven process, with the critical chemical potential for the onset of buckling marked by the red circle.

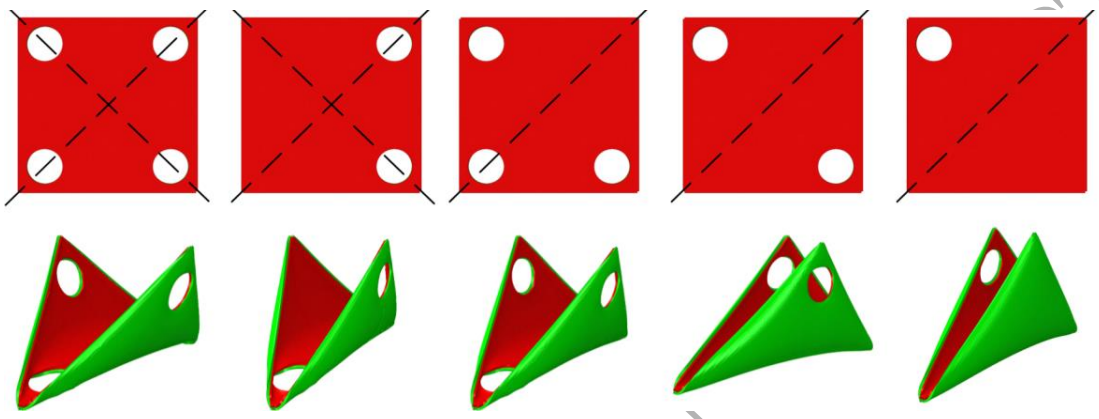

FIG.3 Self-folding of a 10×10mm square bilayer with small circular corner holes with radii 11mm. Top: schematic of the location of the corner holes with black dashed lines the possible folding lines; bottom: simulated folding patterns corresponding to the top bilayers with corner holes.

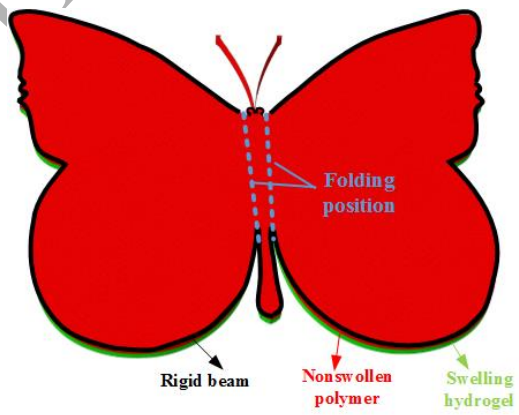

(a)

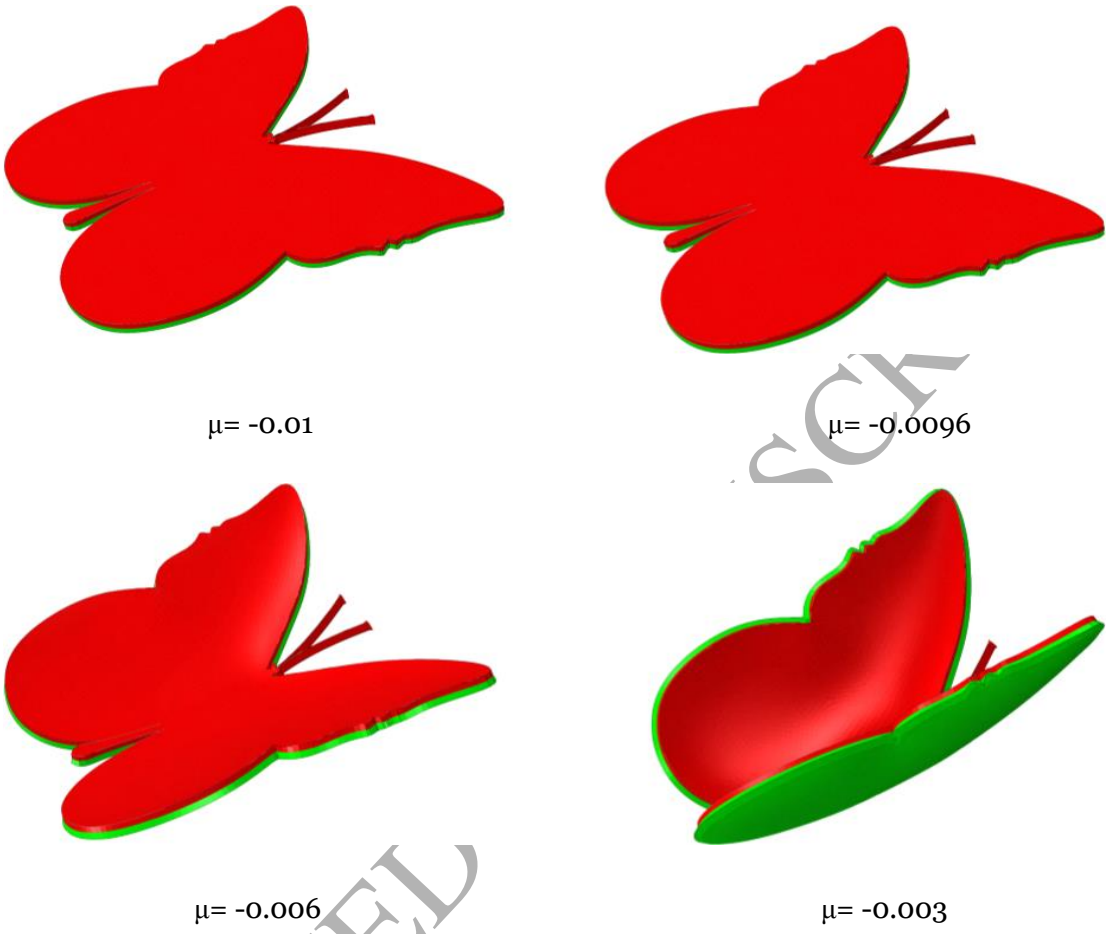

(b)

FIG.4 Self-folding of a butterfly. (a) Designed butterfly shaped hydrogel bilayer with hydrogel layer, polymer film, and rigid beams on the boundary. Dashed lines are the lines where folding occurs. (b) Folding process of the butterfly under various chemical potentials.

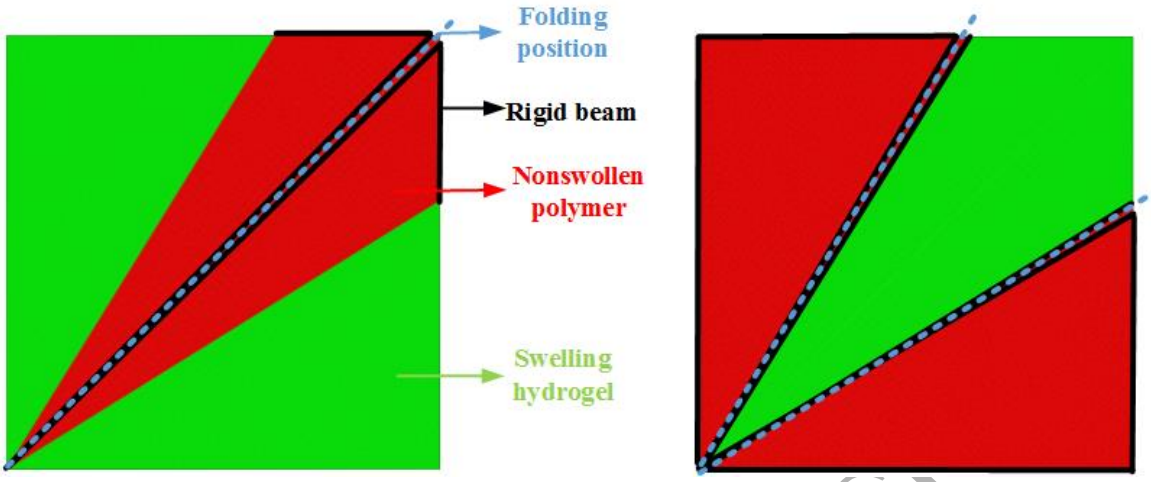

Top view

Bottom view

(a)

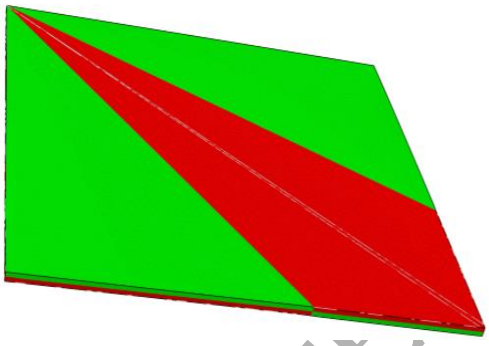

μ= -0.01

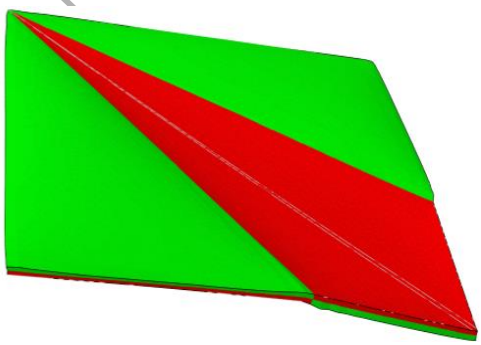

μ= -0.007

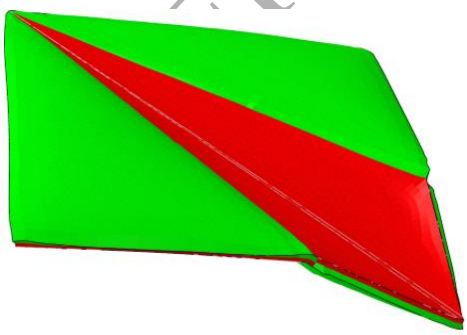

μ= -0.002

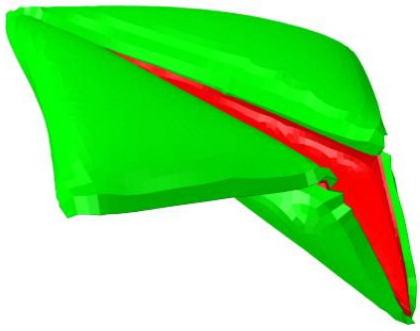

μ= 0

(b)

FIG.5 Origami-inspired self-folding of a paper airplane. (a) Material distribution and design of folding lines. Left: top view, right: bottom view. (b) Folding process of the airplane origami under various chemical potentials.

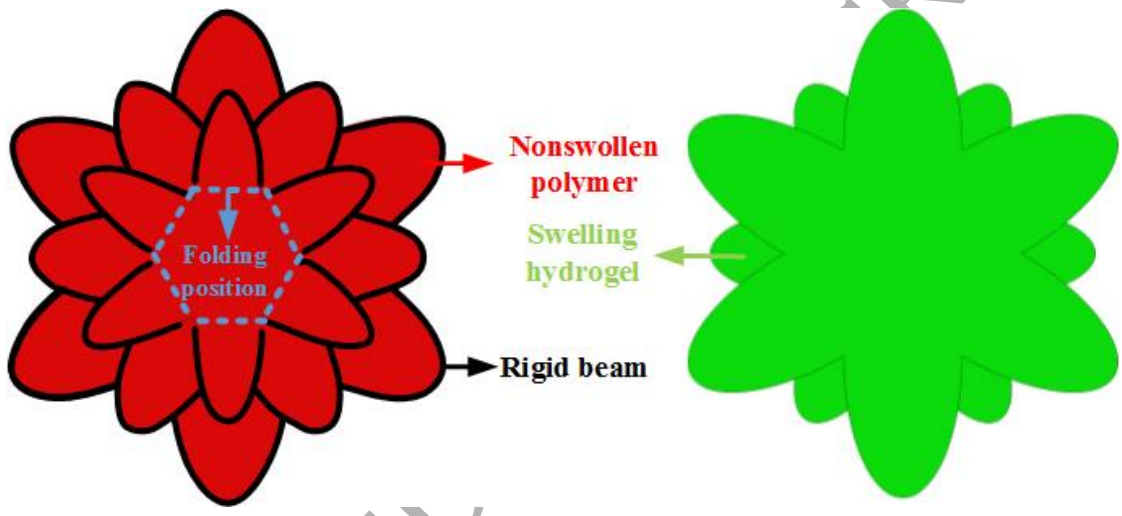

Top view Bottom view

(a)

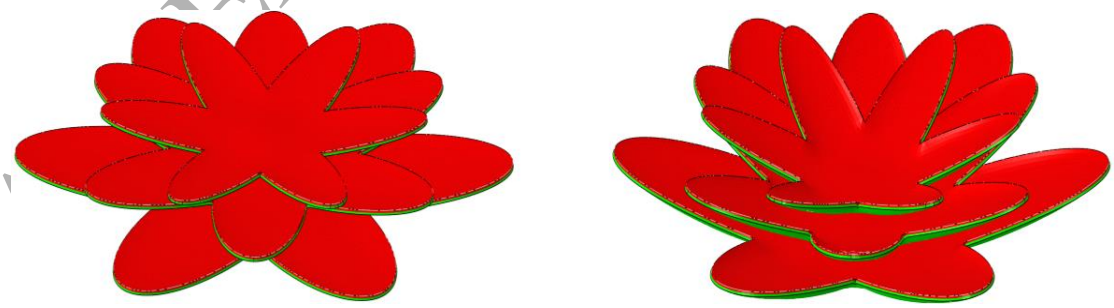

μ= -0.01 μ= -0.005

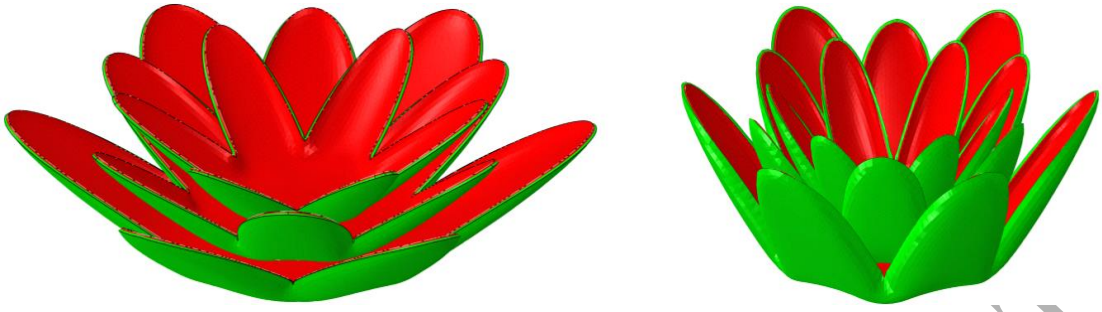

μ= -0.003 μ= -0.001

(b)

FIG.6 Closing of a multi-layer flower. (a) Material distribution and design of folding lines. Left: top view, right: bottom view. (b) Closing process of a multi-layer flower under various chemical potentials.

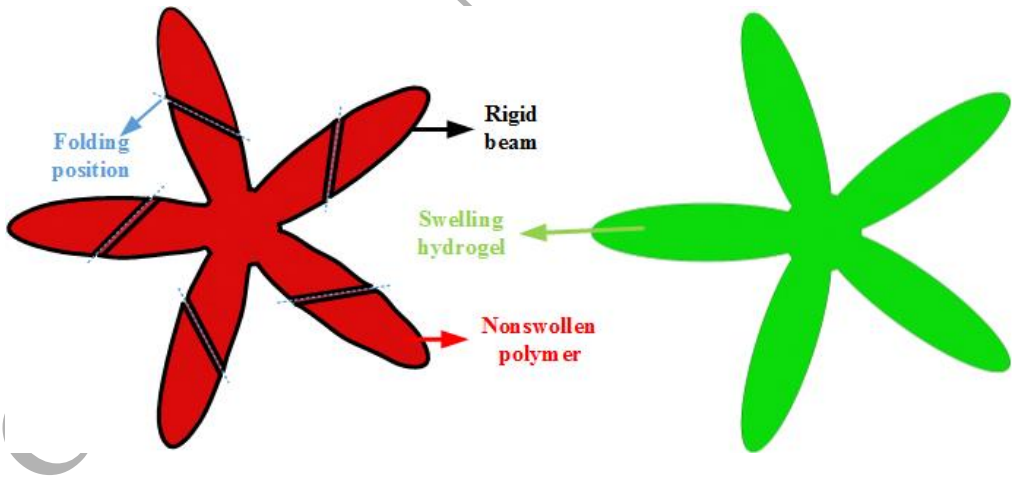

Top view Bottom view

(a)

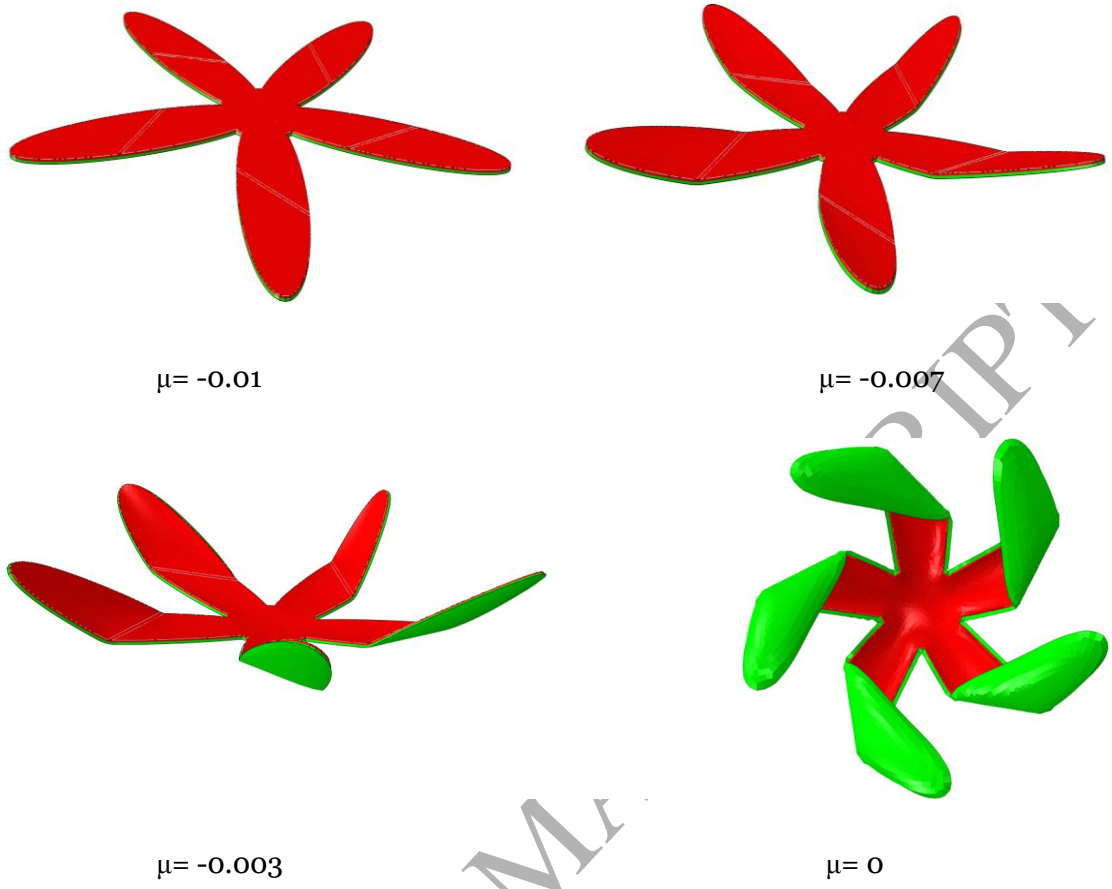

(b)

FIG.7 Self-folding of a propeller. (a) Material distribution and design of folding lines. Left: top view, right: bottom view. (b) Folding process of a propeller under various chemical potentials.

Graphical abstract

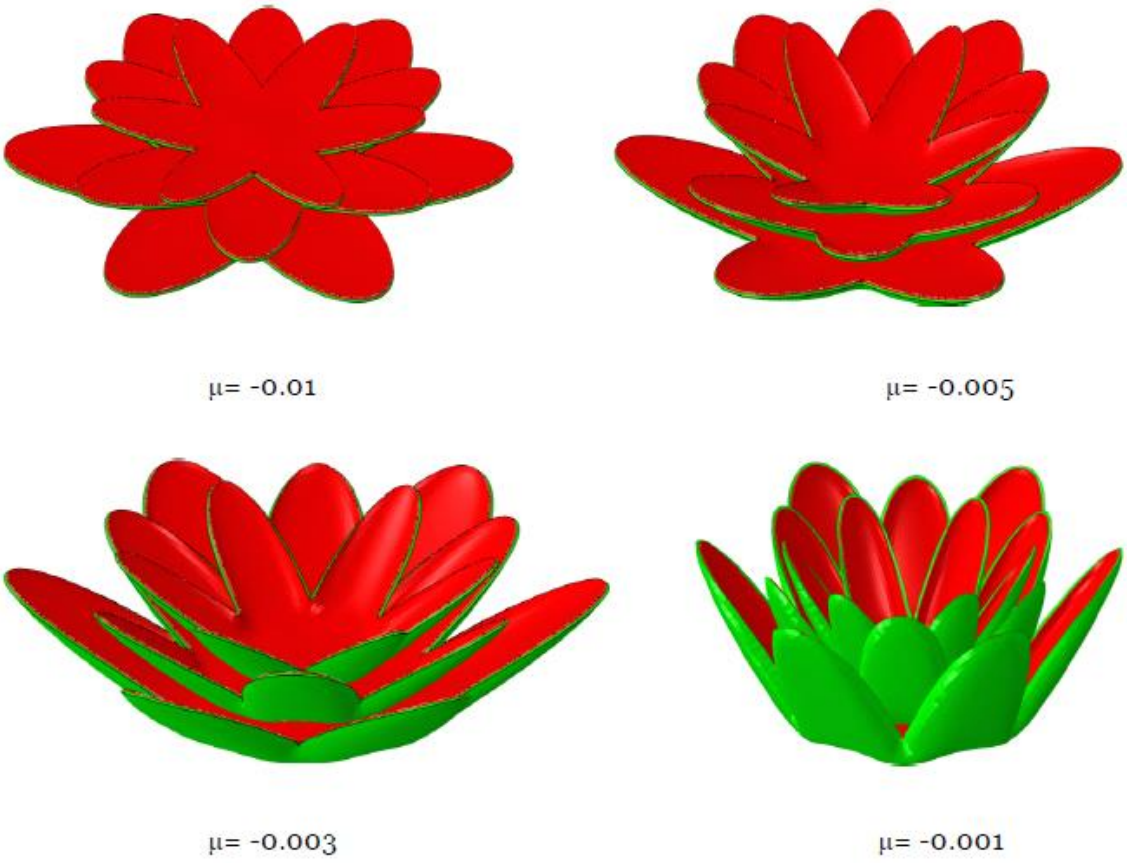

Closing process of a multi-layer flower under various chemical potentials.